

# On using large scale correlation of the Ly- $\alpha$ forest and redshifted 21-cm signal to probe HI distribution during the post reionization era

Tapomoy Guha Sarkar,<sup>a</sup> Kanan K. Datta<sup>b</sup>

<sup>a</sup>Birla Institute of Technology and Science, Pilani - 333031, India

<sup>b</sup>Department of Physics, Presidency University, 86/1 College Street, Kolkata - 700073, India

E-mail: [tapomoy@pilani.bits-pilani.ac.in](mailto:tapomoy@pilani.bits-pilani.ac.in), [kanan.physics@presiuniv.ac.in](mailto:kanan.physics@presiuniv.ac.in)

**Abstract.** We investigate the possibility of detecting the 3D cross correlation power spectrum of the Ly- $\alpha$  forest and HI 21 cm signal from the post reionization epoch. The cross-correlation signal is directly dependent on the dark matter power spectrum and is sensitive to the 21-cm brightness temperature and Ly- $\alpha$  forest biases. These bias parameters dictate the strength of anisotropy in redshift space. We find that the cross-correlation power spectrum can be detected using 400 hrs observation with SKA-mid (phase 1) and a futuristic BOSS like experiment with a quasar (QSO) density of  $30 \text{ deg}^{-2}$  at a peak SNR of 15 for a single field experiment at redshift  $z = 2.5$ . We also study the possibility of constraining various bias parameters using the cross power spectrum. We find that with the same experiment  $1\sigma$  conditional errors on the 21-cm linear redshift space distortion parameter  $\beta_T$  and  $\beta_{\mathcal{F}}$  corresponding to the Ly- $\alpha$  forest are  $\sim 2.7\%$  and  $\sim 1.4\%$  respectively for 10 independent pointings of the SKA-mid (phase 1). This prediction indicates a significant improvement over existing measurements. We claim that the detection of the 3D cross correlation power spectrum will not only ascertain the cosmological origin of the signal in presence of astrophysical foregrounds but will also provide stringent constraints on large scale HI biases. This provides an independent probe towards understanding cosmological structure formation.

---

## Contents

<b>1</b>	<b>Introduction</b>	<b>1</b>
<b>2</b>	<b>Formulation</b>	<b>3</b>
2.1	The Ly- $\alpha$ forest and redshifted 21 cm signal from the post-reionization epoch	3
2.2	Cross-correlation power spectrum	5
2.3	Variance of the estimator and Fisher Matrix analysis	6
<b>3</b>	<b>Results</b>	<b>8</b>
3.1	Power spectrum and its detection	8
3.2	Constraining parameters	12
<b>4</b>	<b>Discussion &amp; Conclusions</b>	<b>14</b>

---

## 1 Introduction

Intensity mapping of the neutral hydrogen (HI) distribution using observations of redshifted 21-cm radiation is a potentially powerful probe of the large scale structure of the universe and the background expansion history the post reionization era [1–4] (also see [5] for a review). The epoch of reionization is believed to be completed by redshift  $z \sim 6$  [6]. Following this era of phase transition, dense self shielded Damped Ly- $\alpha$  (DLA) systems contain bulk of the HI gas. These DLA systems are believed to be the dominant source of the HI 21-cm signal in the post reionization era. Mapping the collective HI 21-cm radiation without resolving the individual DLAs is expected to yield enormous astrophysical and cosmological information regarding the large scale matter distribution, galaxy formation, and expansion history of the Universe in the post-reionization era [4, 7–10].

In the same epoch, HI in the dominantly ionized inter galactic medium (IGM) produces distinct absorption features in the spectra of background QSOs [11]. The Ly- $\alpha$  forest, maps out the HI density fluctuation field along one dimensional skewers which correspond to QSO sight lines. On suitable large cosmological scales both the Ly- $\alpha$  forest and the redshifted 21-cm signal are, however, believed to be biased tracers of the underlying dark matter (DM) distribution [12–15]. Hence, the clustering property of these signals is directly related to the dark matter power spectrum and the cosmological parameters. Like the HI 21-cm signal, Ly- $\alpha$  forest observations also find a host of cosmological applications such as measurement of matter power spectrum [16], cosmological parameters [17, 18], limits on neutrino mass [19], constraints on the dark energy [20], reionization history [21] etc. Several Radio interferometric arrays like the Giant Metrewave Radio Telescope (GMRT) <sup>1</sup>, the Ooty Wide Field Array (OWFA) [22], the Canadian Hydrogen Intensity Mapping Experiment (CHIME) <sup>2</sup>, the Meer-Karoo Array Telescope (MeerKAT) <sup>3</sup>, the Square Kilometer Array (SKA) <sup>4</sup> are being designed and are aimed towards observing the background 21-cm radiation for astrophysical and cosmological investigations. On the other hand, there has been the recent Baryon

---

<sup>1</sup><http://gmrt.ncra.tifr.res.in/>

<sup>2</sup><http://chime.phas.ubc.ca/>

<sup>3</sup><http://www.ska.ac.za/meerkat/>

<sup>4</sup><https://www.skatelescope.org/>

Oscillation Spectroscopic Survey (BOSS) <sup>5</sup> aimed towards probing dark energy and cosmic acceleration through measurements of the large scale structure and the BAO signature in the Ly- $\alpha$  forest [23]. The availability of high signal to noise ratio (SNR) Ly- $\alpha$  forest spectra for a large number of QSOs from the BOSS survey allows 3D statistics to be done with Ly- $\alpha$  forest data [24, 25].

Detection of these signals with high statistical significance is confronted by several observational challenges. For the HI 21-cm observations, the signal is extremely weak intrinsically as compared to the large foregrounds from galactic and extra-galactic sources [26–28]. This inhibits a simple detection. Further, calibration errors and man made radio frequency interferences plague the signal. A statistical detection of the signal requires careful analysis of observational errors and precise subtraction of the foregrounds [29, 30]. The various difficulties faced by Ly- $\alpha$  observations include proper modeling and subtraction of the continuum, flux, incorporating the fluctuations of the ionizing source, uncertainties in the IGM temperature-density relation [31] and contamination of the spectra by metal lines [32].

The two signals being tracers of the underlying large scale structure are expected to be correlated on large scales. However foregrounds and other systematics from two distinct experiments are believed to be uncorrelated between the two independent observations. Hence, the cross correlation signal if detected is more likely to ascertain its cosmological origin. The 2D and 3D cross correlation of the HI 21-cm signal with other tracers of the large scale structure such as the Ly- $\alpha$  forest and the Lyman break galaxies have been proposed as a way to avoid some of the observational issues [33, 35]. The effectiveness of the cross-correlation technique has been demonstrated by successful detection of the HI 21-cm emission at redshift  $\sim 0.8$  using cross correlations of HI 21-cm maps and galaxies [36]. It is important to note that the foregrounds in HI 21-cm observations appear as noise in the cross correlation and hence, a certain degree of foreground cleaning is still required for a statistically feasible detection.

The study of large scale correlation of Ly- $\alpha$  forest [25] has reinforced the belief that the Ly- $\alpha$  forest traces the dark matter. Further, the cross correlation of DLAs and Ly- $\alpha$  forest has been used to measure the DLA bias [37]. While CMBR observations have been able to precisely constrain the cosmological parameters, a study of the neutral IGM requires strong constraints on the bias parameters. These biases are largely investigated in numerical simulations. Recent measurement of Ly- $\alpha$  forest parameters using the BOSS survey [25] is found to be significantly different from those obtained from simulation [12]. Precise constraints on these parameters are extremely important towards understanding the nature of clustering of the IGM and the physics of structure formation. This motivates us to investigate the possibility of measuring large scale HI bias using the cross-correlation of the Ly- $\alpha$  forest with 21-cm signal from the post-reionization epoch.

In this paper we first consider the 3D cross power spectrum of the HI 21-cm maps and large scale Ly- $\alpha$  forest. We discuss the possibility of detecting the signal using the upcoming SKA-mid phase1 (SKA1-mid) like telescopes and future Ly- $\alpha$  forest surveys with very high QSO number densities. Finally we consider the possibility of estimating cosmological parameters using such measurements. The fiducial model is chosen to be the  $\Lambda$ CDM spatially flat cosmology with parameters taken from the WMAP 7 [38]. The cosmological parameter  $\Omega_\Lambda$  is the only free parameter for a flat  $\Lambda$ CDM model. We choose this along with the redshift space parameters for the 21-cm signal and Ly- $\alpha$  observations. Further, the global amplitude of the cross-power spectrum is sensitive to the HI neutral fraction in the post reionization epoch and

---

<sup>5</sup><https://www.sdss3.org/surveys/boss.php>

is chosen as a free parameter. Noting that cosmological parameters are well constrained from CMBR data, our primary focus in this work is to investigate how the upcoming observations may put constraints on the bias parameters for the Ly- $\alpha$  forest and 21-cm signal.

## 2 Formulation

### 2.1 The Ly- $\alpha$ forest and redshifted 21 cm signal from the post-reionization epoch

In the post reionization epoch, small fluctuations in the HI density field in the IGM which is largely ionized, reveal as distinct absorption features in the spectra of background QSOs known as the Ly- $\alpha$  forest. Here, the quantity of observational interest is the transmitted flux  $\mathcal{F}$  through the Ly- $\alpha$  forest. The gas is believed to trace the underlying dark matter distribution [12, 25] on large scales where pressure plays a minor role. The neutral fraction is also assumed to be maintained at a constant value in the IGM owing to photo-ionization equilibrium. This leads to a power law temperature-density relation [39, 40]. These assumptions are incorporated in the fluctuating Gunn-Peterson approximation [41] relating the transmitted flux to the dark matter over-density  $\delta$  as,

$$\frac{\mathcal{F}}{\bar{\mathcal{F}}} = \exp(-\tau) = \exp \left[ -A(1 + \delta)^{2-0.7(\gamma-1)} \right] \quad (2.1)$$

where  $(\gamma - 1)$  denotes the slope of the power law temperature-density relation [31, 40] and is sensitive to the reionization history of the Universe. The parameter  $A \sim 1$  [32] varies with redshift and depends on a host of astrophysical and cosmological parameters, like the photo-ionization rate, IGM temperature, and parameters controlling the background cosmological evolution [16]. It is however reasonable to assume that  $\delta_{\mathcal{F}} = (\mathcal{F}/\bar{\mathcal{F}} - 1) \propto \delta$  with the assumption that the Ly- $\alpha$  forest spectrum has been smoothed over some reasonably large length scale [42, 43]. This linearized relation facilitates analytic computation of the statistical properties of  $\delta_{\mathcal{F}}$ . We note that dominant corrections to this on small scales come from peculiar velocities.

The range of redshifts that can be probed using the Ly- $\alpha$  forest can also be probed using the HI 21-cm emission signal. However, unlike the Ly- $\alpha$  forest which arises from the low density HI residing in the IGM, the 21-cm emission from the same epoch will be dominated by DLAs which are believed to contain most of the HI during the post reionization era. Nevertheless, HI 21-cm signal is likely to trace the underlying DM distribution on large scales of our interest. We use  $\delta_T$  to denote the redshifted 21-cm brightness temperature fluctuations.

We write  $\delta_{\mathcal{F}}$  and  $\delta_T$  in Fourier space as

$$\delta_a(\mathbf{r}) = \int \frac{d^3\mathbf{k}}{(2\pi)^3} e^{i\mathbf{k}\cdot\mathbf{r}} \Delta_a(\mathbf{k}). \quad (2.2)$$

where  $a = \mathcal{F}$  and  $T$  refer to the Ly- $\alpha$  forest transmitted flux and 21-cm brightness temperature respectively. With all the assumptions discussed above and incorporating the effect of peculiar motion through the redshift space distortion, we may write

$$\Delta_a(\mathbf{k}) = C_a[1 + \beta_a\mu^2]\Delta(\mathbf{k}) \quad (2.3)$$

where  $\Delta(\mathbf{k})$  is the dark matter density contrast in Fourier space and  $\mu$  is the cosine of the angle between the line of sight direction  $\hat{\mathbf{n}}$  and the wave vector ( $\mu = \hat{\mathbf{k}} \cdot \hat{\mathbf{n}}$ ).  $\beta_a$  is the linear redshift distortion parameter.

For the 21-cm brightness temperature field we have

$$C_T = 4.0 \text{ mK } b_T \bar{x}_{\text{HI}} (1+z)^2 \left( \frac{\Omega_{b0} h^2}{0.02} \right) \left( \frac{0.7}{h} \right) \left( \frac{H_0}{H(z)} \right) \quad (2.4)$$

where  $\bar{x}_{\text{HI}}$  is the mean neutral fraction. The neutral hydrogen fraction is assumed to be a constant with a value  $\bar{x}_{\text{HI}} = 2.45 \times 10^{-2}$  obtained from the measurement of  $\Omega_{gas} \sim 10^{-3}$  [45–48]. In the case of HI 21-cm signal the parameter  $\beta_T$ , which is known as linear redshift distortion parameter, can be written as the ratio between the growth rate of linear perturbations  $f(z)$  and the HI bias  $b_T$ . The bias function  $b_T(k, z)$  has an intrinsic scale dependence below the Jeans scale and an implicit scale dependence arising from the fluctuations in the ionizing background [2]. Moreover, it has been shown [44] that this bias is a monotonically growing function of redshift. The assumption of linear bias is supported by numerical simulations [13, 14] which indicate that over a wide range of scales, a constant bias model is adequate to describe the distribution of neutral gas for  $z < 3$ . Recent measurement of DLA bias is also consistent with the constant bias model [37]. We find that  $f(z) \approx 1$  at the fiducial redshift of interest  $z = 2.5$ . We adopt a constant bias  $b_T = 2$  which is consistent with recent results from numerical simulations of HI 21-cm signal in the post-reionization epoch [13–15]. This gives the value of the parameter  $\beta_T \approx 0.5$ .

The linear distortion parameter for the Ly- $\alpha$  forest, denoted by  $\beta_{\mathcal{F}}$ , can not be interpreted in the same way as  $\beta_T$ . This is because of the non-linear relationship between the observed Ly- $\alpha$  transmitted flux and the underlying DM density field [25]. The bias factor for the forest is the bias of the contrast of the fluctuations in the flux and is not same as the HI bias. Unlike the HI 21-cm signal, the parameters  $(C_{\mathcal{F}}, \beta_{\mathcal{F}})$  are independent of each other and are dependent on the model parameters  $A, \gamma$  and the flux probability distribution function (PDF) of the Ly- $\alpha$  forest. In the absence of primordial non-gaussianity, fluctuations in the Ly- $\alpha$  flux can be well described by a linear theory with a scale independent bias on large scales. This is supported by numerical simulations [12]. The values of  $\beta_{\mathcal{F}}$  obtained in particle-mesh (PM) simulations demonstrate that simulations with lower resolution (larger smoothing length) yield lower values of  $\beta_{\mathcal{F}}$ . The smoothing scale is ideally set by the Jean’s scale which is sensitive to the temperature history of the IGM.

We adopt an approximate values  $(C_{\mathcal{F}}, \beta_{\mathcal{F}}) \approx (-0.15, 1.11)$  from the numerical simulations of Ly- $\alpha$  forest [12]. We note that for cross-correlation studies the Ly- $\alpha$  forest has to be smoothed to the resolution of the HI 21 cm frequency channels. On these smoothed scales the linear bias model is well tested in simulations. Results of full hydrodynamical simulations are expected to yield information at smaller scales which are not necessary for the present analysis. We, however, note that these bias values have large uncertainties owing to the lack of accurate modeling of the IGM. The redshift space distortion parameter  $\beta_{\mathcal{F}}$ , is also sensitive to the probing redshift. The large scale correlation of Ly- $\alpha$  transmitted flux from BOSS survey [25] shows that the parameters  $(C_{\mathcal{F}}, \beta_{\mathcal{F}})$  are significantly different from the above values obtained from simulations. However it has been suggested that metal line contamination and correct treatment of DLAs may explain this discrepancy. In this paper we shall stick to the values obtained from simulation [12].

## 2.2 Cross-correlation power spectrum

The possibility that both the Ly- $\alpha$  forest and the HI 21-cm signal from the post reionization epoch trace the underlying dark matter density field on large scales, motivates us to investigate their cross-correlation signal [33]. Though the respective auto-correlation power spectra can independently put constraints on various astrophysical and cosmological parameters there are several advantages of cross-correlating the signals.

The main advantage of cross-correlation is that the issue of foregrounds and other systematics can be coped with greater ease as compared to the auto correlation. Even the smallest foreground residual will plague the auto-correlation signal. The cosmological origin of the signal can only be ascertained if it is detected with statistical significance in cross-correlation. Further, a joint analysis of two data sets would involve not only the individual auto-correlation but also the cross-correlation information. Sometimes the two independent probes focus on specific complimentary Fourier modes with high SNR whereby the cross signal takes advantage of both the probes simultaneously. This has been studied in the context of BAO where, owing to the difference in values of the parameters  $\beta_T$  and  $\beta_{\mathcal{F}}$  the two probes have different sensitivities to radial and transverse clustering [34].

It is true that if the observations of the independent probes are perfect measurements no new information can be obtained from the cross correlation. However, the first generation measurements of the HI 21 cm signal are expected to be noisy and shall have systematic errors. For a detection of the 21 cm signal these measurements can in principle be cross-correlated against a high SNR Ly- $\alpha$  forest signal for cosmological investigations which may not be possible with the low quality auto correlation analysis.

We consider the power spectrum of 21-cm signal, the Ly- $\alpha$  forest and the cross correlation power spectrum in three dimensions. The general 3-D power spectra for the two fields are defined as

$$\langle \Delta_a(\mathbf{k})\Delta_b^*(\mathbf{k}') \rangle = (2\pi)^3 \delta^3(\mathbf{k} - \mathbf{k}') P_{ab}(\mathbf{k}) \quad (2.5)$$

where  $a, b$  can be  $\mathcal{F}$  and  $T$ . In general the power spectrum can be written in redshift space as,

$$P_{ab}(\mathbf{k}) = C_a C_b (1 + \beta_a \mu^2)(1 + \beta_b \mu^2) P(\mathbf{k}) \quad (2.6)$$

where  $P(\mathbf{k})$  is the matter power spectrum. The auto-correlation power spectrum corresponds to  $a = b$  and the cross-correlation power spectrum corresponds to  $a \neq b$ .

The cross-correlation can be computed only in the region of overlap between the observed Ly- $\alpha$  forest and 21-cm fields. However, we note that in real observations the Ly- $\alpha$  forest surveys are likely to cover much larger volume than the single field radio observations of the HI 21-cm signal. We consider such an overlap volume  $\mathcal{V}$  consisting of a patch of angular extent  $\theta_a \times \theta_a$  on the sky plane and of thickness  $L$  along the line of sight direction. We consider the flat sky approximation. This amounts to writing the comoving separation vector  $\mathbf{r}$  as

$$\mathbf{r} = r_\nu \vec{\theta} + \hat{\mathbf{n}} \frac{dr}{d\nu} \nu \quad (2.7)$$

where  $r_\nu$  is the comoving distance corresponding to the observing frequency  $\nu$  and  $\vec{\theta}$  is a 2D vector on the sky plane. If  $B$  denotes the bandwidth of the 21-cm observation, we have  $L = B dr/d\nu$  and  $\mathcal{V} = r_\nu^2 \theta_a^2 L$ . The observed 21-cm signal (after significant foreground cleaning) in Fourier space is written as

$$\Delta_{T_o}(\mathbf{k}) = \Delta_T(\mathbf{k}) + \Delta_{NT}(\mathbf{k}), \quad (2.8)$$

where  $\Delta_{NT}$  is the corresponding noise. The radio observations measure visibilities as a function of the 2D baseline vector  $\mathbf{U}$  and frequency  $\nu$ . We have  $\mathbf{k} = (\mathbf{k}_\perp, k_\parallel) = (2\pi\mathbf{U}/r_\nu, 2\pi\tau d\nu/dr)$  where  $\tau$  is the Fourier conjugate variable corresponding to  $\nu$ . The 21-cm brightness temperature fluctuations in Fourier space are closely related to the measured Visibilities.

The Ly- $\alpha$  flux fluctuations are written as a field in the 3-D space as  $\delta_{\mathcal{F}}(\mathbf{r})$ . In reality one has the observed quantity  $\delta_{\mathcal{F}o}(\mathbf{r})$  which consists of the continuous field sampled along skewers corresponding to QSO sight lines. We, hence have  $\delta_{\mathcal{F}o}(\mathbf{r}) = \delta_{\mathcal{F}}(\mathbf{r}) \times \rho(\mathbf{r})$ , where the sampling function  $\rho(\mathbf{r})$  is defined as

$$\rho(\mathbf{r}) = \frac{\sum_i w_i \delta_D^2(\mathbf{r}_\perp - \mathbf{r}_{\perp a})}{L \sum_i w_i} \quad (2.9)$$

and is normalized to unity ( $\int dV \rho(\mathbf{r}) = 1$ ). The index ' $i$ ' goes up to  $N_Q$ , the total number of QSOs considered. The weights  $w_i$  introduced in the definition of  $\rho$  are chosen so as to minimize the variance. The suitable choice of the  $w_i$  takes care of the fact that the pixel noise for each of the QSO spectra are in principle different. We have, in Fourier space,

$$\Delta_{\mathcal{F}o}(\mathbf{k}) = \tilde{\rho}(\mathbf{k}) \otimes \Delta_{\mathcal{F}}(\mathbf{k}) + \Delta_{N\mathcal{F}}(\mathbf{k}), \quad (2.10)$$

where  $\tilde{\rho}$  is the Fourier transform of  $\rho$ ,  $\otimes$  denotes a convolution and  $\Delta_{N\mathcal{F}}(\mathbf{k})$  denotes a noise term.

We define the cross-correlation estimator  $\hat{\mathcal{E}}$  as

$$\hat{\mathcal{E}} = \frac{1}{2} [\Delta_{\mathcal{F}o}(\mathbf{k}) \Delta_{T_o}^*(\mathbf{k}) + \Delta_{\mathcal{F}o}^*(\mathbf{k}) \Delta_{T_o}(\mathbf{k})]. \quad (2.11)$$

We are interested in the statistical properties of this estimator. Using the definitions of  $\Delta_{\mathcal{F}o}(\mathbf{k})$  and  $\Delta_{T_o}(\mathbf{k})$ , we obtain the expectation value of  $\hat{\mathcal{E}}$ . Simple algebraic manipulation yields

$$\langle \hat{\mathcal{E}} \rangle = P_{\mathcal{F}T}(\mathbf{k}). \quad (2.12)$$

Thus, the estimator is unbiased and its expectation value faithfully returns the quantity we are probing, namely the 3-D cross-correlation power spectrum  $P_{\mathcal{F}T}(\mathbf{k})$ . We have assumed that the different noises are uncorrelated. Further, we note that the QSOs are distributed at a redshift different from rest of the quantities and hence  $\tilde{\rho}$  shall be uncorrelated with both  $\Delta_T$  and  $\Delta_{\mathcal{F}}$ .

### 2.3 Variance of the estimator and Fisher Matrix analysis

The variance of the estimator  $\hat{\mathcal{E}}$ , defined as,  $\sigma_{\hat{\mathcal{E}}}^2 = \langle \hat{\mathcal{E}}^2 \rangle - \langle \hat{\mathcal{E}} \rangle^2$  gives

$$\begin{aligned} \sigma_{\hat{\mathcal{E}}}^2 &= \frac{1}{2} P_{\mathcal{F}T}(\mathbf{k})^2 + \frac{1}{2} [P_{\mathcal{F}\mathcal{F}}(\mathbf{k}) + P_{\mathcal{F}\mathcal{F}}^{1D}(k_\parallel) P_w^{2D} + N_{\mathcal{F}}] \\ &\quad \times [P_{TT}(\mathbf{k}) + N_T]. \end{aligned} \quad (2.13)$$

The quantity  $P_{\mathcal{F}\mathcal{F}}^{1D}(k_\parallel)$  is known as the aliasing term and is the usual 1-D Ly- $\alpha$  flux power spectrum of the individual spectra given by

$$P_{\mathcal{F}\mathcal{F}}^{1D}(k_\parallel) = \frac{1}{(2\pi)^2} \int d^2\mathbf{k}_\perp P_{\mathcal{F}\mathcal{F}}(\mathbf{k}). \quad (2.14)$$

The quantity  $P_w^{2D}$  denotes the power spectrum of the weight function. The quantities  $N_T$  and  $N_{\mathcal{F}}$  denote the effective noise power spectra for the 21-cm and Ly- $\alpha$  observations respectively. Writing  $\mathbf{k} = (\mathbf{k}_\perp, k_\parallel)$  with  $|\mathbf{k}_\perp| = k_\perp = k \sin \theta$  and  $k_\parallel = k \cos \theta$ , we have

$$\delta P_{\mathcal{F}T}(\mathbf{k}) = \frac{\sigma_{\hat{\epsilon}}}{\sqrt{N_m(k, \theta)}} \quad (2.15)$$

where  $N_m(k, \theta)$  is number of observable modes in between  $k$  to  $k + dk$  and  $\theta$  to  $\theta + d\theta$  given by

$$N_m(k, \theta) = \frac{2\pi k^2 \mathcal{V} \sin \theta dk d\theta}{(2\pi)^3}. \quad (2.16)$$

For the Ly- $\alpha$  forest one may choose the weights  $w_i$  of the inverse variance form [49]. However, an uniform weighing scheme suffices when most of the spectra are measured with a sufficiently high SNR [50]. This gives  $P_w^{2D} = \frac{1}{\bar{n}}$ , where  $\bar{n}$  is the 2D density of QSOs ( $\bar{n} = N_Q/\mathcal{A}$ ). We assume that the variance  $\sigma_{\mathcal{F}N}^2$  of the pixel noise contribution to  $\delta_{\mathcal{F}}$  is the same across all the QSO spectra whereby we have  $N_{\mathcal{F}} = \sigma_{\mathcal{F}N}^2/\bar{n}$  for its noise power spectrum. In arriving at equation (2.13) we have ignored the effect of QSO clustering. In reality, the distribution of QSOs is expected to exhibit clustering. The clustering would enhance the term  $(P_{\mathcal{F}\mathcal{F}}^{1D}(k_\parallel)P_w^{2D} + N_{\mathcal{F}})$  in equation (2.13) by a factor  $(1 + \bar{n}C_Q(\mathbf{k}_\perp))$ , where  $C_Q(\mathbf{k}_\perp)$  is the angular power spectrum of the QSOs. However, for the QSO surveys under consideration, the Poisson noise dominates over the clustering term and the latter may be ignored.

We consider a radio-interferometric measurement of the 21-cm signal whereby the instrumental sensitivity per ( $k$ ) mode to the redshifted 21-cm power spectrum at an observed frequency  $\nu = 1420/(1+z)$  MHz can be calculated using the relation [51]

$$N_T(k, \nu) = \frac{T_{sys}^2}{Bt_0} \left( \frac{\lambda^2}{A_e} \right)^2 \frac{r_\nu^2 L}{n_b(U, \nu)}. \quad (2.17)$$

Here,  $T_{sys}$  denotes the system temperature.  $B$  and  $L$  are, as described before, the observation bandwidth and comoving length corresponding to the bandwidth  $B$  respectively,  $t_0$  is the total observation time,  $r_\nu$  is the comoving distance to the redshift  $z$ ,  $n_b(U, \nu)$  is the number density of baseline  $U$ , where  $U = k_\perp r_\nu/2\pi$ , and  $A_e$  is the effective collecting area for each individual antenna. We may write  $n_b(U, \nu)$  as

$$n_b(U, \nu) = \frac{N(N-1)}{2} f_{2D}(U, \nu), \quad (2.18)$$

where  $N$  is the total number of antennae in the radio array and  $f_{2D}(U, \nu)$  is the normalized baseline distribution function which follows the normalization condition  $\int d^2\mathbf{U} f_{2D}(U, \nu) = 1$ . The Ly- $\alpha$  forest flux and the 21-cm signal are modeled using parameters  $(C_\alpha, \beta_\alpha)$ . The quantity  $A = C_T C_{\mathcal{F}}$  appears as a single overall constant and is largely uncertain. We note that the parameter  $C_\alpha$  also includes the bias parameter  $b_\alpha$ . Additionally, we consider the possibility of constraining this amplitude, two linear redshift space distortion parameters i.e,  $\beta_T$  and  $\beta_F$  along with the cosmological parameter  $\Omega_\Lambda$  assuming a flat  $\Lambda$ CDM model i.e,  $\Omega_\Lambda + \Omega_m = 1$ . We label these 4 parameters as  $\lambda_r$ . The Fisher matrix used for estimation of parameters is given by the  $4 \times 4$  matrix

$$F_{rs} = \int \int \frac{1}{\sigma_{\hat{\epsilon}}^2} \left( \frac{\partial P_{\mathcal{F}T}}{\partial \lambda_r} \right) \left( \frac{\partial P_{\mathcal{F}T}}{\partial \lambda_s} \right) \frac{2\pi \mathcal{V} k^2 dk d\mu}{(2\pi)^3}, \quad (2.19)$$



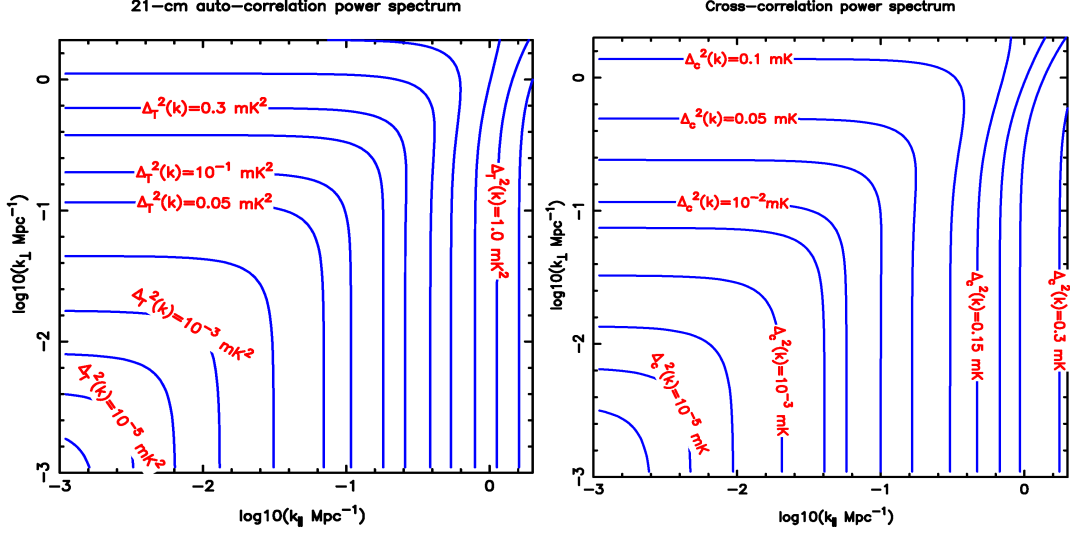


**Figure 1.** Figure shows the 3D power spectrum in redshift space at a fiducial redshift  $z = 2.5$ . The left panel shows the 21-cm power spectrum  $\Delta_T^2 = k^3 P_{TT}(\mathbf{k})/2\pi^2$  and the right panel shows the cross-correlation power spectrum  $\Delta_C^2 = k^3 P_{T\mathcal{F}}(\mathbf{k})/2\pi^2$ . The redshift space distortion appears as deviations from spherical symmetry of the power spectrum.

where  $\sigma_{\mathcal{E}}$  is obtained from equation (2.13). The marginalized error on the  $i^{\text{th}}$  parameter  $\Delta\lambda_i$  is given by the Cramer-Rao bound;  $\Delta\lambda_i = \sqrt{F_{ii}^{-1}}$ .

This gives the theoretical bound for the error in a given parameter. If the errors are correlated, then in the space of the parameters we shall have error contours corresponding to the significance at which statistical detection is sought. Assuming the Cramer-Rao bound, the error contours are expected to be elliptic whose areas measure the figure of merit, and the orientation of the principal axis measures the strength of correlation between the parameters.

### 3 Results

#### 3.1 Power spectrum and its detection

The left panel of the figure (1) shows the dimensionless 21-cm power spectrum ( $\Delta_T^2(k_{\perp}, k_{\parallel}) = k^3 P_T(k_{\perp}, k_{\parallel})/2\pi^2$ ) in redshift space at the fiducial redshift  $z = 2.5$ . In the range of modes of interest  $10^{-2} \lesssim k \lesssim 1 \text{ Mpc}^{-1}$  the signal varies in the range  $10^{-3} \lesssim \Delta_T^2 \lesssim 1 \text{ mK}^2$ . We find that in the plane of  $k_{\parallel}$  and  $k_{\perp}$  the power spectrum is not circularly symmetric. The degree of asymmetry is sensitive to the redshift space distortion parameter. Thus, for a given  $k$ -mode the power spectrum differs for different sets of  $(k_{\perp}, k_{\parallel})$  values. The right panel of figure (1) shows the 21-cm and Ly- $\alpha$  cross-power spectrum. The departure from spherical symmetry is noted here as well. However, the magnitude and scale dependence of the distortion is different from the 21-cm auto power spectrum owing to the difference between the linear distortion parameters  $\beta$  for Ly- $\alpha$  forest and the 21-cm signal. We note that anisotropies in the power spectrum are determined by linear distortion parameters  $\beta$ . The quantity  $\beta_F$  is  $\sim 3$  times larger than  $\beta_T$ . Hence, the cross-correlation power spectrum is more anisotropic than the HI 21-cm auto correlation power spectrum. The cross correlation signal varies in the range  $10^{-4} \lesssim \Delta_c^2 \lesssim 10^{-1} \text{ mK}$  in the  $k$ -range  $10^{-2} \lesssim k \lesssim 1 \text{ Mpc}^{-1}$ .

We have chosen a fiducial redshift of  $z = 2.5$  for our analysis. This is justified since the QSO distribution is known to peak in the redshift range  $2 < z < 3$ . Further, to avoid metal line contamination and the effect of the QSO Stromgren sphere, only a part of the QSO spectra is to be considered. At the fiducial redshift this corresponds to approximately a redshift band  $\Delta z \sim 0.4$ . The cross-correlation can however only be computed in the region of overlap between the 21-cm signal and the Ly- $\alpha$  forest field. This is dictated by whichever is smaller - the band width of the 21-cm signal or the redshift range over which one has the Ly- $\alpha$  spectra.

The details of the radio interferometer specifications used here, other than the baseline distribution function can be found in a recent paper [15]. In brief, we consider a radio interferometric array for the 21-cm observations mimicking the SKA1-mid. The SKA1-mid is one of the three different instruments that will be built as a part of the SKA telescope. Although these specifications may undergo changes, we use the specifications provided in the ‘Baseline Design Document’<sup>6</sup>.

We now describe the telescope specifications used for our analysis. We consider an operational frequency range of 350 MHz to 14 GHz. We assume a total of 250 dish like antennae each of  $\sim 15$ m diameter<sup>7</sup>. To calculate the normalized baseline distribution function  $f_{2D}(U, \nu)$  we use the baseline density provided in [35] (blue line in their Fig. 6). The blue line is essentially proportional to  $f_{2D}(U)$  for a given frequency  $\nu$ . We use the normalization condition  $\int d^2\mathbf{U} f_{2D}(U, \nu) = 1$  to calculate the normalization factor. We note that the baseline distribution is centrally condensed with 40%, 55%, 70%, and 100% of the total antennae are within 0.35 km, 1 km, 2.5 km, and 100 km radius respectively. We also assume that there is no baseline coverage below 30m. Centrally condensed baseline coverage helps to achieve sufficient power spectrum sensitivity at large scales. The coverage is poor at very small scales (large  $U$ ). However, owing to non-linear effects the modeling of the power spectrum at these small scales is anyway quite incomplete. We plug everything in Eq. 2.17 to obtain the required noise error in the 21 cm power spectrum for a given  $(k_{\perp}, k_{\parallel})$ . Then, for a given bin  $(k_{\perp} + dk_{\perp}, k_{\parallel} + dk_{\parallel})$  we calculate the total number of independent modes  $N_c$  and reduce the noise rms. by a factor of  $\sqrt{N_c}$ . We assume  $T_{sys}$  to be 30K for the redshifts  $z = 2.5$  corresponding to observational frequency of 405.7 MHz. We also consider observations over 32 MHz bandwidth and a typical antenna efficiency equal to 0.7.

We note that for a QSO at a given redshift, the region  $10,000 \text{ km s}^{-1}$  blue-wards of the QSO’s Ly- $\alpha$  emission has to be excluded from the Ly- $\alpha$  forest to avoid the QSO’s proximity effect. Further, at least  $1,000 \text{ km s}^{-1}$  red-ward of the QSO’s Ly- $\beta$  and O-VI lines may be discarded to avoid any confusion with the Ly- $\beta$  forest or the intrinsic O-VI absorption. For example a QSO at a fiducial redshift 2.5, this would allow the Ly- $\alpha$  forest to be measured in the redshift range  $1.96 \leq z \leq 2.39$  spanning an interval  $\Delta z = 0.43$ . It is necessary to consider a survey with a higher QSO density for the cross correlation SNR to be competitive with that of the 21-cm auto-correlation. We consider a BOSS-like QSO survey with a QSO density of  $30 \text{ deg}^{-2}$  which are measured at average  $2\sigma$  sensitivity. Though the QSO surveys

<sup>6</sup>available here: <https://www.skatelescope.org/key-documents/>

<sup>7</sup> A recent document “SKA Level 1 Requirements (revision 6)” (<https://www.skatelescope.org/key-documents/>) has indicated that only  $\sim 50\%$  of these antennae may be deployed. To achieve the same level of accuracy presented in this work with this degraded design one has to approximately consider 4 times the total observation time projected in this paper. However, this is a naive scaling and redesigned baseline distribution may change the entire analysis. For example, if the reduction is only of the large baseline antennae then the sensitivities presented here may not be that severely affected.

cover a large portion of the sky,  $\sim 10,000\text{deg}^2$ , the cross correlation can only be computed in the region of overlap of the 21-cm and Ly- $\alpha$  forest survey.

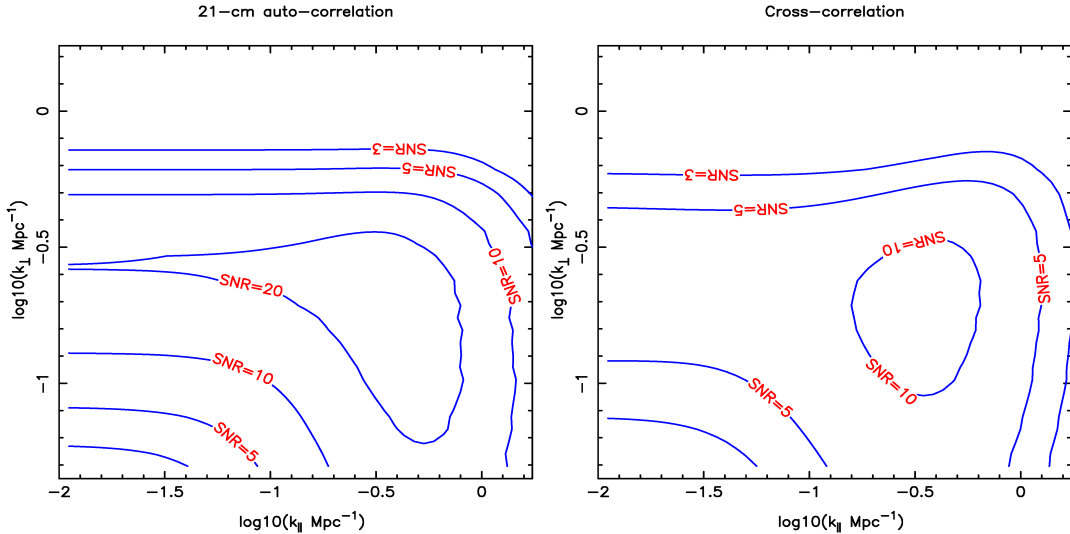


**Figure 2.** SNR contours for the 21-cm auto-correlation (left panel) and the cross correlation (right panel) power spectrum in redshift space at the fiducial redshift  $z = 2.5$  for a 400hrs observation at 405MHz assuming that complete foreground removal is done.

We first consider the idealized situation where the foregrounds in the 21-cm observations are completely absent. This means that a perfect foreground subtraction has been achieved. The left panel of the figure (2) shows the SNR contours for the 21-cm auto correlation power spectrum for a 400 hrs observation and total 32MHz bandwidth at a frequency 405.7 MHz corresponding to  $z = 2.5$  in this idealized situation. We have taken a bin size to be  $(\Delta k, \Delta\theta) = (k/5, \pi/10)$ . The SNR reaches at the peak ( $> 20$ ) at intermediate value of  $(k_{\perp}, k_{\parallel}) = (0.4, 0.4) \text{Mpc}^{-1}$  and falls off at both lower and higher  $k$ -values. We find that  $5\sigma$  is possible in the range  $0.08 \lesssim k_{\perp} \lesssim 0.6 \text{Mpc}^{-1}$  and  $0.1 \lesssim k_{\parallel} \lesssim 1.5 \text{Mpc}^{-1}$ . The similar range for the  $10\sigma$  detection is  $0.12 \lesssim k_{\perp} \lesssim 0.5 \text{Mpc}^{-1}$  and  $0.2 \lesssim k_{\parallel} \lesssim 1.2 \text{Mpc}^{-1}$ . At lower values of  $k$ , the noise is dominated by cosmic variance whereas, the noise is predominantly instrumental at large  $k$ . However, lower cut-off for the  $k_{\parallel}$  arises from the limited bandwidth which we assume to be 32 MHz in this work. The presence of redshift space distortion shows up as an asymmetry in the sensitivity contours in the  $(k_{\parallel}, k_{\perp})$  plane. The enhanced radial clustering due to redshift space distortion effect manifests as higher SNR (say  $> 10$ ) for a larger range of  $k_{\parallel}$  than  $k_{\perp}$ .

The right panel of the figure (2) shows the SNR contours in the  $(k_{\parallel}, k_{\perp})$  plane for the Ly- $\alpha$  forest 21-cm cross-correlation power spectrum. For the 21 cm signal, a 400 hrs observation is considered. We have considered a QSO number density of  $\bar{n} = 30\text{deg}^{-2}$ , and the Ly- $\alpha$  spectra are assumed to be measured at a  $2\sigma$  sensitivity level. We use  $\beta_F$  to be 1.11 and overall normalization factor  $C_F = -0.15$  consistent with recent measurement [25]. The spectra is assumed to be smoothed to the same level as the frequency channel width of the 21 cm observations and the cross correlation is computed in the region of overlap between the two fields. Although the overall SNR for the cross correlation power spectrum is lower as compared to the 21-cm auto correlation power spectrum, a  $5\sigma$  detection is possible in the range  $0.1 \lesssim k_{\perp} \lesssim 0.4 \text{Mpc}^{-1}$  and  $0.1 \lesssim k_{\parallel} \lesssim 1 \text{Mpc}^{-1}$ . The SNR peaks ( $> 10$ ) at

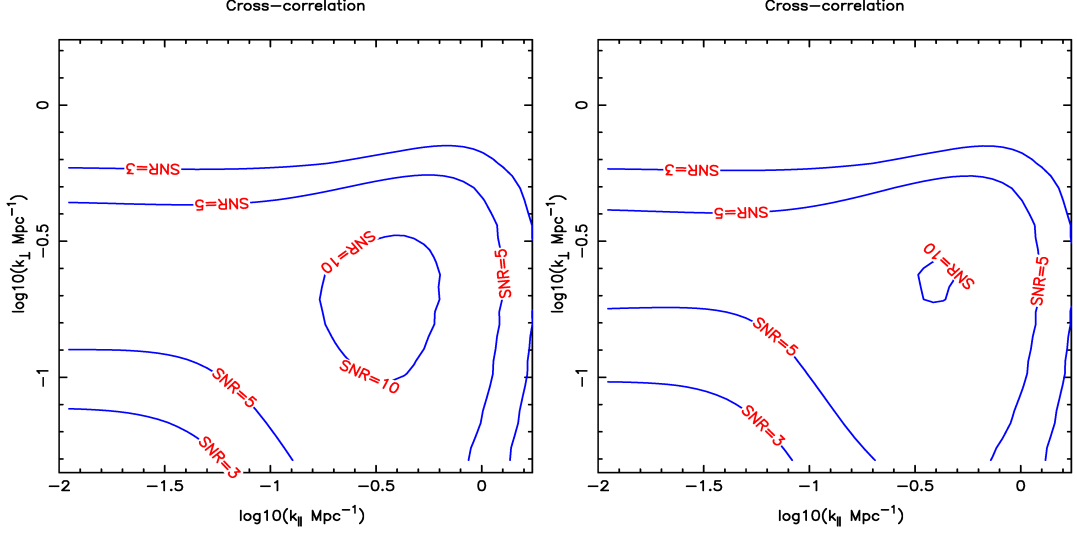


**Figure 3.** SNR contours for the cross power spectrum in redshift space at the fiducial redshift  $z = 2.5$  for a 400hrs observation at 405MHz with 10% (left) and 100% (right) foreground residuals remaining in the 21-cm signal.

$(k_{\perp}, k_{\parallel}) \sim (0.2, 0.3) \text{ Mpc}^{-1}$ . We find that in the variance budget  $\sigma_{\hat{\theta}}^2$  (eq. 2.13) the second term always dominates over the first term and therefore the variance is essentially determined by the second term. In an ideal situation when the system noise for HI 21-cm ( $N_T$ ) and Ly- $\alpha$  forest ( $N_{\mathcal{F}}$ ) are zero or negligible, and  $\bar{n}$  is large such that the term  $P_{\mathcal{F}\mathcal{F}}^{1D}(k_{\parallel})P_w^{2D}$  becomes very small, the two terms in the rhs. of eq. 2.13 become comparable. This is the cosmic variance limited. However, in practice the second term is always significantly larger than the first term except at very large scales. We further notice that the second term, which dominates the variance budget in almost all scales, is actually determined by the  $P_{\mathcal{F}\mathcal{F}}^{1D}(k_{\parallel})P_w^{2D}$  (which arises due to the discreteness of QSO sight-lines) and the system noise in HI 21-cm survey i.e,  $N_T$ . To be precise, we find that  $P_{\mathcal{F}\mathcal{F}}^{1D}(k_{\parallel})P_w^{2D}$  dominates over  $P_{\mathcal{F}\mathcal{F}}(\mathbf{k})$  for the scales  $(k_{\perp}, k_{\parallel}) \gtrsim (0.05, 0.1) \text{ Mpc}^{-1}$ . Similarly  $N_T$  is higher than  $P_{TT}$  for the scales  $(k_{\perp}, k_{\parallel}) \gtrsim (0.2, 0.3) \text{ Mpc}^{-1}$ . The variance can be reduced either by increasing the QSO number density or by increasing the observing time for HI 21-cm survey. The QSO number density considered here is already on the higher side for the BOSS like survey. Therefore, the only viable way to reduce the variance is to consider more observation time for HI 21-cm survey.

It is important to note the role of foreground residuals in auto and cross-correlation. Whereas foregrounds appear as an inseparable contaminant to the auto-correlation signal, they appear only as a contribution to the noise in the cross correlation. In the computation of SNR for auto-correlation we have tacitly assumed that the foregrounds can be distinguished from the true cosmological signal. This is practically not possible and any foreground residual will plague the signal with additional power which has no cosmological significance. The figure 2 is in fact hypothetical since it assumes that foregrounds can be distinguished and completely separated from the signal. This issue is however not present in the cross signal. Any foreground residual in the 21 cm observation shall only degrade the noise and not affect the cross correlated signal. This is a key advantage of using cross-correlation as a cosmological probe as any detection here will ascertain the cosmological origin of the signal.

The figure 3 shows the cross-correlation in a more realistic scenario wherein we consider the inclusion of foreground residuals. Though the scale dependence of foreground residual may differ significantly from that of the signal we have modeled foreground residuals as merely 10% and 100% of the signal to get a rough order of magnitude estimate about the degradation of SNR in the presence of foreground residuals. We note that the  $k$ -dependence of the contours here significantly depends on the nature and clustering properties of the foregrounds and is also dependent on the foreground subtraction technique. We find that a peak SNR of 16 and 12 respectively can be achieved for these cases respectively. We find that the degradation of the peak SNR is not significant when the foreground residual is 10% of the signal. However, we note that (see the right panel of Figure 3) when foreground residuals are as large as 100% of the signal, there is approximately 35% reduction of the SNR as compared to the no-foreground case. The presence of a 100% foreground residuals will clearly inhibit its detection using the 21-cm auto-correlation power spectrum. However, we can see that a statistically significant detection with high SNR is possible using the cross-correlation even if the foreground residual is  $\sim 100\%$  of the HI 21-cm signal.

### 3.2 Constraining parameters

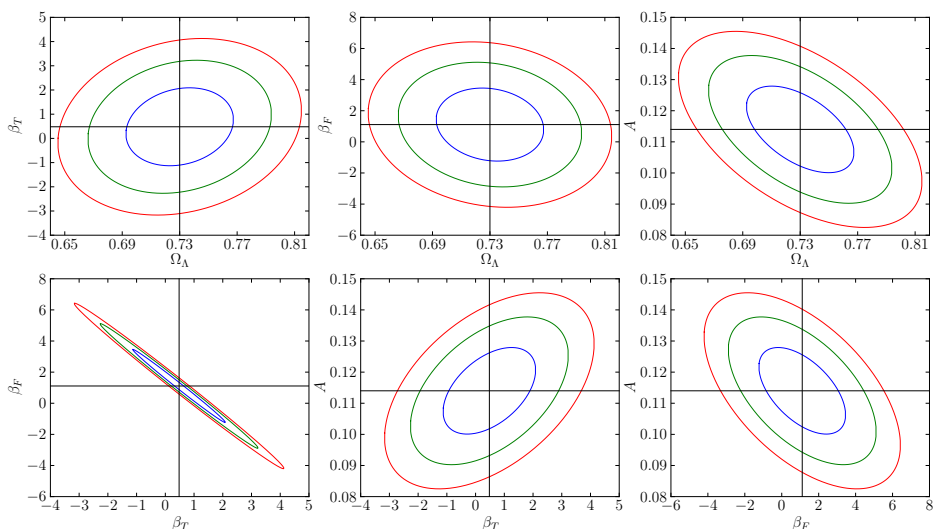


**Figure 4.** Showing the 68.3%, 95.4% and 99.8% confidence contours for the parameters  $(A, \beta_T, \beta_{\mathcal{F}}, \Omega_\Lambda)$ .

We shall now consider the possibility of constraining various model parameters using the Fisher matrix analysis. Figure (4) shows the 68.3%, 95.4% and 99.8% confidence contours obtained using the Fisher matrix analysis for the parameters  $(A, \beta_T, \beta_{\mathcal{F}}, \Omega_\Lambda)$ . The table 1 shows the  $1 - \sigma$  error for the above parameters. Owing to the smallness of the contribution of the redshift space distortion to the power spectrum, the parameters  $\beta_{\mathcal{F}}$  and  $\beta_T$  are rather badly constrained and errors are very large. The parameters  $(\Omega_\Lambda, A)$  are constrained much better at (3.5%, 8%) respectively. The parameter  $A$  is proportional to  $b_T x_{\text{HI}} C_{\mathcal{F}}$ . Hence, the constraint on  $A$  is implicitly related to the constraint on the mean neutral fraction. The projections presented here are for a single field of view radio observation.

The full coverage of a typical Ly- $\alpha$  survey covers much larger volume and several beams of the radio observation shall fit in this. The noise scales as  $\sigma/\sqrt{N}$  where  $N$  is the number of pointings. Such enhancement of the volume shall allow the constraints to get much tighter. Figure 5 shows the marginalized one dimensional probability distribution function (PDF) for  $\beta_T$  and  $\beta_F$  corresponding to 10 pointings. This gives an error on the parameters which are roughly of the same order of magnitude as the fiducial values itself. The marginalized errors can however be reduced by considering more pointings.

**Table 1.** This shows  $1 - \sigma$  error on various parameters for a single field observation.

Parameters	Fiducial Value	$1\sigma$ Error (marginalized)	$1\sigma$ Error (conditional)
$\beta_T$	0.48	1.06	0.04
$\beta_{\mathcal{F}}$	1.11	1.55	0.05
$\Omega_\Lambda$	0.73	0.025	0.013
$A$	0.114	0.01	0.002

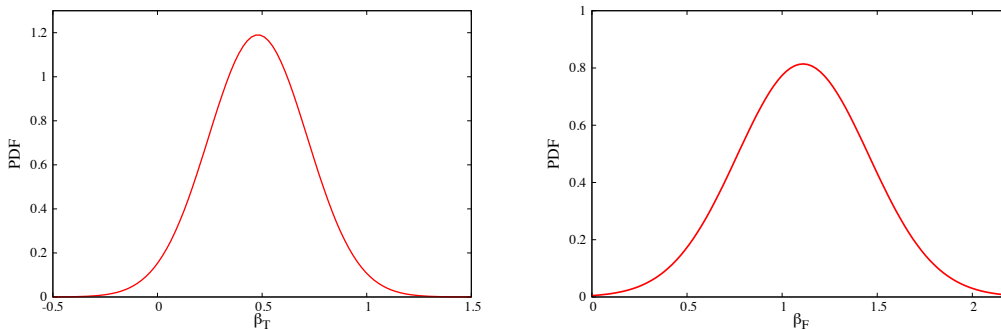


**Figure 5.** Figure shows the marginalized one dimensional probability distribution function (PDF) for  $\beta_T$  and  $\beta_F$  corresponding to 10 pointings.

Till now we have assumed that all the four parameters ( $A, \beta_T, \beta_{\mathcal{F}}, \Omega_\Lambda$ ) are unknown. In the estimation of the parameters we have treated them as four free parameters. We find that the constraints on  $\beta_T$  and  $\beta_{\mathcal{F}}$  are rather poor even if we consider 10 independent pointings of radio observations. We now consider error on each parameter assuming that the other three are known. This gives us the conditional error on each parameter. The conditional  $1 - \sigma$  error in  $\beta_T$  and  $\beta_{\mathcal{F}}$  are 8.5% and 4.5% respectively for single pointing radio observation. For 10 independent radio observations the conditional errors improve to 2.7%, 1.4%, 0.4% and 0.6% for  $\beta_T, \beta_{\mathcal{F}}, \Omega_\Lambda$  and  $A$  respectively. We note that these conditional errors give the best theoretical bounds on the parameters for the given observational specifications. These constraints obtained on redshift space distortion parameters  $\beta$  from our cross-correlation analysis is better as compared to the existing constraints [25, 37] and competitive with other cosmological probes aiming towards the same measurements. Further, higher density of QSOs and enhanced SNR for the individual QSO spectra shall also ensure more stringent constraints.

## 4 Discussion & Conclusions

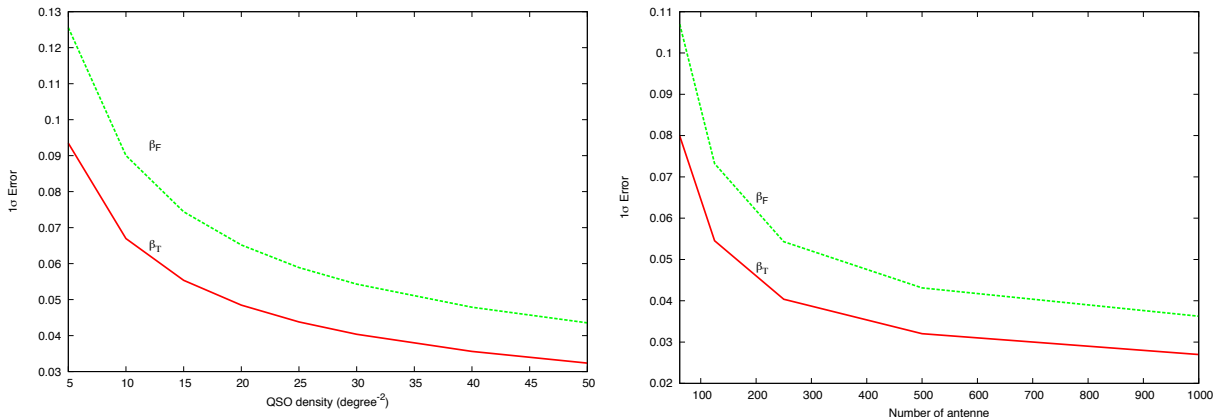


**Figure 6.** The left and right panels show  $1\sigma$  conditional errors on parameters  $\beta_T$  and  $\beta_F$  as a function of QSO number density  $\bar{n}$  (left) and number of antennae (right) for total observing time  $t_{obs} = 400$  hrs and  $\bar{n} = 30 \text{ deg}^{-2}$  respectively for a single field radio observation. We note that the total collecting area of the telescope increases linearly with increase in the number of antennae. All other parameters are kept fixed.

Our analysis has so far focused on estimates obtained for specific HI 21-cm intensity mapping (with SKA1-mid) and Ly- $\alpha$  forest (with BOSS) experiments. We shall now discuss how these estimates vary for various other possible experiments.

We first consider the effect of QSO number density on the constraints on the redshift space distortion parameters. Fig 6 (left) shows  $1\sigma$  conditional errors on redshift space distortion parameters  $\beta_T$  and  $\beta_F$  as a function of QSO number density  $\bar{n}$  for a total observing time  $t_{obs} = 400$  hrs for a single field radio observation. All other observational parameters are held fixed. We find that there is a significant improvement in the constraints with increase in the QSO number density. This improvement in the constraints is expected to saturate at very high QSO number density. However, obtaining QSO number density  $\bar{n} > 50 \text{ deg}^{-2}$  with high SNR is unfeasible in near future and therefore we do not explore that possibility. The right panel of Fig. 6 shows  $1\sigma$  conditional errors on parameters  $\beta_T$  and  $\beta_F$  as a function of number of antennae for  $\bar{n} = 30 \text{ deg}^{-2}$ . The total collecting area of the telescope increases linearly with increase in the number of antennae. The SKA telescope is in design phase and any degradation of baseline distribution through reduction of the proposed number of antennae will affect the constraints on  $\beta_T$  and  $\beta_F$  according to the Figure 6. We find a considerable improvement in the constraints when the total number of antennae increases from 62 to 500, beyond which we hardly notice any improvement. Based on this, we argue that an increase in the number of antennae beyond 500 for the SKA1-mid like experiments is unlikely to improve constraints on redshift space distortion parameters. We note that the SKA telescope is in design phase and any degradation of baseline distribution through reduction of the proposed number of antennae will affect the constraints on  $\beta_T$  and  $\beta_F$  according to the Figure 6.

An important feature of radio interferometer design is the array configuration which determines the baseline distribution  $f_{2D}(U, \nu)$ . In the previous section we considered the baseline distribution function for the SKA1-mid. We now consider three other baseline distribution corresponding to radially symmetric antenna distribution of the form  $\sim r^{-n}$

**Table 2.** This shows  $1-\sigma$  **conditional** error on various parameters for different baseline distributions.

Parameters	SKA1-mid	n=1	n=2	n=3
$\beta_T$	0.04	0.037	0.032	0.032
$\beta_{\mathcal{F}}$	0.05	0.049	0.044	0.044
$\Omega_\Lambda$	0.013	0.012	0.011	0.011
$A$	0.002	0.002	0.0018	0.0018

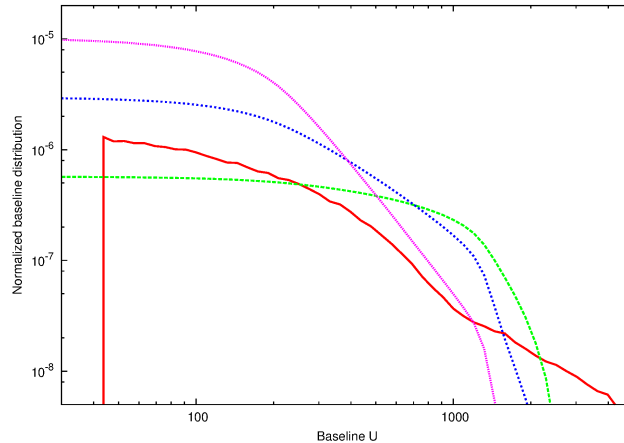


**Figure 7.** The normalized baseline distribution function  $f_{2D}(U, \nu)$ . The solid curve shows the normalized baseline distribution for the SKA1-mid. The other three curves correspond to power law antenna distribution with power law indices  $n = 3, 2, 1$  (top to bottom).

with  $n = 1, 2, 3$ . We assume that the array has a uniform antenna distribution up to a radius of 80m. We also assume that all the antennae are confined within a radius of 1 km. Fig. 7 shows the normalized baseline distribution function for these cases.

We wish to study the role of the compactness of the radio array on parameter estimation. The  $1\sigma$  conditional errors for these baseline distribution functions are summarized in Table 2. We find that there is a general improvement of our results as compared to the SKA1-mid when all the antennae are confined within a radius of 1 km. We note that for the SKA1-mid, about 50% of the antennae are outside the 1 km core where as all antennae are confined within a radius of 1 km for the above three array designs. We find that there is a slight improvement in the constraints when the power law index is varied from  $n = 1$  to 2. But, hardly any improvement is noticed when the index is changed from  $n = 2$  to  $n = 3$ .

It is clear that distributing antennae at large distances in such experiments (where resolution is not a prime concern) is not advantageous since at large baselines the signal is sub-dominant. On the contrary it is useful to consider arrays in which most antennae are packed within a small radius. However, we note that an arbitrary compactification (from  $n = 2$  to 3) of the array causes us to lose  $k$ -modes which contribute to the signal and there is no further improvement in the SNR.

It is important to choose the optimal observational strategy for the 21-cm signal. One may consider a deep observation (long time of observation) in a single field of view as opposed



to the possibility of dividing the same total observation time over many pointings. We know that on large scales the dominant contribution to noise comes from the cosmic variance. This can only be mitigated by increasing the survey volume. Deep observations in a small patch of the sky is not beneficial for reducing the cosmic variance. Observing multiple fields ensures that both the system noise contribution and the cosmic variance for the cross-correlation is reduced. The noise in this case is reduced on all scales. However, if one considers an observation for the same total time but in a single field of view, the system noise contribution indeed reaches the same minimum value but the noise which is dominated by the cosmic variance on large scales does not get reduced. It is thus strategically better for cross-correlation measurements to consider observations in multiple fields.

The issue of foreground subtraction, though less severe for the cross-correlation is still a major concern for the 21-cm signal. Astrophysical foregrounds from galactic and extra galactic sources plague the signal [29] and significant amount of foreground subtraction is required before the cross-correlation is performed. The foregrounds appear as noise in the cross-correlation and may be tackled by considering larger number of Fourier modes (larger volumes). Similarly, for the Ly- $\alpha$  forest observations, continuum subtraction and avoiding metal line contamination, though less problematic, has to be performed with extreme precision. Moreover, man made radio frequency interferences (RFIs), calibration errors and other systematics pose a serious threat to the detection of the HI 21-cm signal. A detailed analysis of these issues is outside the scope of the present work. We intent to address these observational aspects in a future work.

Finally, this work emphasizes the important role of using cross correlation to bypass the fundamental problem posed by 21-cm foregrounds towards its detection through auto-correlation. We have shown that the 3D cross-correlation power spectrum from the post reionization epoch as a direct probe of cosmological structure formation can be detected to a high level of statistical sensitivity with telescopes such as the SKA. We have also focused on the possibility of constraining the bias (redshift space distortion) parameters for the 21-cm signal and the Ly- $\alpha$  forest. This investigation is crucial towards understanding the nature of HI bias in two distinct astrophysical systems under consideration namely Ly- $\alpha$  forest (diffuse low density HI in the IGM) and 21-cm signal (clumped HI in DLAs). These biases are studied extensively in numerical simulations. It is important for observational constraints to be compared with the simulation results to support their validity. Modeling of the IGM is incomplete without the precise knowledge about HI bias. In the absence of high quality 21-cm data it is important to make predictions based on future experiments. We find that strong constraints may be obtained on  $(\beta_T, \beta_{\mathcal{F}})$  from advanced BOSS and SKA like experiments.

We conclude by noting that the cross-correlation of the Ly- $\alpha$  forest and the HI 21 cm signal as an independent probe of astrophysics and cosmology may allow us to put strong constraints on redshift space distortion parameters towards important understanding and modeling of the post reionization HI distribution.

## Acknowledgements

The authors would like to thank Anjan Sarkar for useful discussion on Fisher matrix analysis. The authors would also like to thank Mario G. Santos for providing them with the SKA1-mid array baseline distribution. TGS would like to acknowledge the Department of Science and Technology (DST), Government of India for providing financial support through the projects SR/FTP/PS-172/2012. KKD would like to thank DST for support

through the project SR/FTP/PS-119/2012 and the University Grant Commission (UGC), India for support through UGC-faculty recharge scheme (UGC-FRP) vide ref. no. F.4-5(137-FRP)/2014(BSR).

## References

- [1] S. Bharadwaj and S. K. Sethi, *HI Fluctuations at Large Redshifts: I-Visibility correlation*, *Journal of Astrophysics and Astronomy* **22** (December, 2001) 293–307, [[astro-ph/0203269](#)].
- [2] J. S. B. Wyithe and A. Loeb, *The 21-cm power spectrum after reionization*, *Monthly Notices of the Royal Astronomical Society* **397** (August, 2009) 1926–1934, [[arXiv:0808.2323](#)].
- [3] A. Loeb and J. S. B. Wyithe, *Possibility of Precise Measurement of the Cosmological Power Spectrum with a Dedicated Survey of 21cm Emission after Reionization*, *Physical Review Letters* **100** (April, 2008) 161301–161310, [[arXiv:0801.1677](#)].
- [4] T. Chang, U. Pen, J. B. Peterson, and P. McDonald, *Baryon Acoustic Oscillation Intensity Mapping of Dark Energy*, *Physical Review Letters* **100** (March, 2008) 091303–091310, [[arXiv:0709.3672](#)].
- [5] M. F. Morales and J. S. B. Wyithe, *Reionization and Cosmology with 21-cm Fluctuations*, *Annual Review of Astronomy & Astrophysics* **48** (September, 2010) 127–171, [[arXiv:0910.3010](#)].
- [6] X. Fan, M. A. Strauss, R. H. Becker, R. L. White, J. E. Gunn, G. R. Knapp, G. T. Richards, D. P. Schneider, J. Brinkmann, and M. Fukugita, *Constraining the Evolution of the Ionizing Background and the Epoch of Reionization with  $z \sim 6$  Quasars. II. A Sample of 19 Quasars*, *The Astronomical Journal* **132** (July, 2006) 117–136, [[astro-ph/0512082](#)].
- [7] J. S. B. Wyithe, *A method to measure the mass of damped Ly $\alpha$  absorber host galaxies using fluctuations in 21-cm emission*, *Monthly Notices of the Royal Astronomical Society* **388** (August, 2008) 1889–1898, [[arXiv:0804.1624](#)].
- [8] S. Bharadwaj, S. K. Sethi, and T. D. Saini, *Estimation of cosmological parameters from neutral hydrogen observations of the post-reionization epoch*, *Physical Review D* **79** (April, 2009) 083538–083542, [[arXiv:0809.0363](#)].
- [9] S. Camera, M. G. Santos, P. G. Ferreira, and L. Ferramacho, *Cosmology on Ultralarge Scales with Intensity Mapping of the Neutral Hydrogen 21 cm Emission: Limits on Primordial Non-Gaussianity*, *Physical Review Letters* **111** (October, 2013) 171302, [[arXiv:1305.6928](#)].
- [10] P. Bull, P. G. Ferreira, P. Patel, and M. G. Santos, *Late-time cosmology with 21cm intensity mapping experiments*, *ArXiv e-prints* (May, 2014) [[arXiv:1405.1452](#)].
- [11] M. Rauch, *The Lyman Alpha Forest in the Spectra of QSOs*, *Annual Review of Astronomy & Astrophysics* **36** (1998) 267–316, [[astro-ph/9806286](#)].
- [12] P. McDonald, *Toward a Measurement of the Cosmological Geometry at  $z \sim 2$ : Predicting Ly- $\alpha$  Forest Correlation in Three Dimensions and the Potential of Future Data Sets*, *Astrophysical Journal* **585** (March, 2003) 34–51, [[astro-ph/0108064](#)].
- [13] J. S. Bagla, N. Khandai, and K. K. Datta, *HI as a probe of the large-scale structure in the post-reionization universe*, *Monthly Notices of the Royal Astronomical Society* **407** (September, 2010) 567–580, [[arXiv:0908.3796](#)].
- [14] T. Guha Sarkar, S. Mitra, S. Majumdar, and T. R. Choudhury, *Constraining large-scale H I bias using redshifted 21-cm signal from the post-reionization epoch*, *Monthly Notices of the Royal Astronomical Society* **421** (April, 2012) 3570–3578, [[arXiv:1109.5552](#)].
- [15] F. Villaescusa-Navarro, M. Viel, K. K. Datta, and T. R. Choudhury, *Modeling the neutral*

- hydrogen distribution in the post-reionization Universe: intensity mapping*, *Journal of Cosmology and Astroparticle Physics* **9** (September, 2014) 50, [[arXiv:1405.6713](#)].
- [16] R. A. C. Croft, D. H. Weinberg, M. Pettini, L. Hernquist, and N. Katz, *The Power Spectrum of Mass Fluctuations Measured from the Ly $\alpha$  Forest at Redshift  $Z=2.5$* , *Astrophysical Journal* **520** (July, 1999) 1–23, [[astro-ph/9809401](#)].
- [17] R. Mandelbaum, P. McDonald, U. Seljak, and R. Cen, *Precision cosmology from the Lyman  $\alpha$  forest: power spectrum and bispectrum*, *Monthly Notices of the Royal Astronomical Society* **344** (September, 2003) 776–788, [[astro-ph/0302112](#)].
- [18] J. Lesgourgues, M. Viel, M. G. Haehnelt, and R. Massey, *A combined analysis of 3D weak lensing, Lyman- $\alpha$  forest and WMAP year three data*, *Journal of Cosmology and Astro-Particle Physics* **11** (November, 2007) 8–15, [[arXiv:0705.0533](#)].
- [19] R. A. C. Croft, W. Hu, and R. Davé, *Cosmological Limits on the Neutrino Mass from the Ly $\alpha$  Forest*, *Physical Review Letters* **83** (August, 1999) 1092–1095, [[astro-ph/9903335](#)].
- [20] P. McDonald and D. J. Eisenstein, *Dark energy and curvature from a future baryonic acoustic oscillation survey using the Lyman- $\alpha$  forest*, *Physical Review D* **76** (September, 2007) 063009–063015, [[astro-ph/0607122](#)].
- [21] S. Gallerani, T. R. Choudhury, and A. Ferrara, *Constraining the reionization history with QSO absorption spectra*, *Monthly Notices of the Royal Astronomical Society* **370** (August, 2006) 1401–1421, [[astro-ph/0512129](#)].
- [22] S. S. Ali and S. Bharadwaj, *Prospects for Detecting the 326.5 MHz Redshifted 21-cm HI Signal with the Ooty Radio Telescope (ORT)*, *Journal of Astrophysics and Astronomy* **35** (June, 2014) 157–182, [[arXiv:1310.1707](#)].
- [23] T. Delubac, J. E. Bautista, N. G. Busca, J. Rich, D. Kirkby, S. Bailey, A. Font-Ribera, A. Slosar, K.-G. Lee, M. M. Pieri, J.-C. Hamilton, E. Aubourg, M. Blomqvist, J. Bovy, J. Brinkmann, W. Carithers, K. S. Dawson, D. J. Eisenstein, J.-P. Kneib, J.-M. Le Goff, D. Margala, J. Miralda-Escudé, A. D. Myers, R. C. Nichol, P. Noterdaeme, R. O’Connell, M. D. Olmstead, N. Palanque-Delabrouille, I. Pâris, P. Petitjean, N. P. Ross, G. Rossi, D. J. Schlegel, D. P. Schneider, D. H. Weinberg, C. Yèche, and D. G. York, *Baryon Acoustic Oscillations in the Ly $\{\alpha\}$  forest of BOSS DR11 quasars*, *ArXiv e-prints* (April, 2014) [[arXiv:1404.1801](#)].
- [24] I. Pâris, P. Petitjean, É. Aubourg, N. P. Ross, A. D. Myers, A. Streblyanska, S. Bailey, P. B. Hall, M. A. Strauss, S. F. Anderson, D. Bizyaev, A. Borde, J. Brinkmann, J. Bovy, W. N. Brandt, H. Brewington, J. R. Brownstein, B. A. Cook, G. Ebelke, X. Fan, N. Filiz Ak, H. Finley, A. Font-Ribera, J. Ge, F. Hamann, S. Ho, L. Jiang, K. Kinemuchi, E. Malanushenko, V. Malanushenko, M. Marchante, I. D. McGreer, R. G. McMahon, J. Miralda-Escudé, D. Muna, P. Noterdaeme, D. Oravetz, N. Palanque-Delabrouille, K. Pan, I. Perez-Fournon, M. Pieri, R. Riffel, D. J. Schlegel, D. P. Schneider, A. Simmons, M. Viel, B. A. Weaver, W. M. Wood-Vasey, C. Yèche, and D. G. York, *The Sloan Digital Sky Survey quasar catalog: tenth data release*, *Astronomy and Astrophysics* **563** (March, 2014) A54, [[arXiv:1311.4870](#)].
- [25] A. Slosar, A. Font-Ribera, M. M. Pieri, J. Rich, J.-M. Le Goff, É. Aubourg, J. Brinkmann, N. Busca, B. Carithers, R. Charlassier, M. Cortês, R. Croft, K. S. Dawson, D. Eisenstein, J.-C. Hamilton, S. Ho, K.-G. Lee, R. Lupton, P. McDonald, B. Medolin, D. Muna, J. Miralda-Escudé, A. D. Myers, R. C. Nichol, N. Palanque-Delabrouille, I. Pâris, P. Petitjean, Y. Piškur, E. Rollinde, N. P. Ross, D. J. Schlegel, D. P. Schneider, E. Sheldon, B. A. Weaver, D. H. Weinberg, C. Yèche, and D. G. York, *The Lyman- $\alpha$  forest in three dimensions: measurements of large scale flux correlations from BOSS 1st-year data*, *Journal of Cosmology and Astroparticle Physics* **9** (September, 2011) 1, [[arXiv:1104.5244](#)].
- [26] M. G. Santos, A. Cooray, and L. Knox, *Multifrequency Analysis of 21 Centimeter Fluctuations from the Era of Reionization*, *Astrophysical Journal* **625** (June, 2005) 575–587, [[astro-ph/0408515](#)].

- [27] T. Di Matteo, R. Perna, T. Abel, and M. J. Rees, *Radio Foregrounds for the 21 Centimeter Tomography of the Neutral Intergalactic Medium at High Redshifts*, *Astrophysical Journal* **564** (January, 2002) 576–580, [[astro-ph/](#)].
- [28] A. Ghosh, S. Bharadwaj, S. S. Ali, and J. N. Chengalur, *GMRT observation towards detecting the post-reionization 21-cm signal*, *Monthly Notices of the Royal Astronomical Society* **411** (March, 2011) 2426–2438, [[arXiv:1010.4489](#)].
- [29] A. Ghosh, S. Bharadwaj, S. S. Ali, and J. N. Chengalur, *Improved foreground removal in GMRT 610 MHz observations towards redshifted 21-cm tomography*, *Monthly Notices of the Royal Astronomical Society* **418** (December, 2011) 2584–2589, [[arXiv:1108.3707](#)].
- [30] D. Alonso, P. Bull, P. G. Ferreira, and M. G. Santos, *Blind foreground subtraction for intensity mapping experiments*, *Monthly Notices of the Royal Astronomical Society* **447** (February, 2015) 400–416, [[arXiv:1409.8667](#)].
- [31] P. McDonald, J. Miralda-Escudé, M. Rauch, W. L. W. Sargent, T. A. Barlow, and R. Cen, *A Measurement of the Temperature-Density Relation in the Intergalactic Medium Using a New Ly $\alpha$  Absorption-Line Fitting Method*, *Astrophysical Journal* **562** (November, 2001) 52–75, [[astro-ph/](#)].
- [32] T. Kim, J. S. Bolton, M. Viel, M. G. Haehnelt, and R. F. Carswell, *An improved measurement of the flux distribution of the Ly $\alpha$  forest in QSO absorption spectra: the effect of continuum fitting, metal contamination and noise properties*, *Monthly Notices of the Royal Astronomical Society* **382** (December, 2007) 1657–1674, [[arXiv:0711.1862](#)].
- [33] T. Guha Sarkar, S. Bharadwaj, T. R. Choudhury, and K. K. Datta, *Cross-correlation of the H I 21-cm signal and Ly $\alpha$  forest: a probe of cosmology*, *Monthly Notices of the Royal Astronomical Society* **410** (January, 2011) 1130–1134, [[arXiv:1002.1368](#)].
- [34] T. Guha Sarkar, S. Bharadwaj, *Predictions for BAO distance estimates from the cross-correlation of the Lyman- $\alpha$  forest and redshifted 21-cm emission*, *Journal of Cosmology and Astro-Particle Physics* **023** (August, 2013), [[arXiv:1002.1368](#)].
- [35] F. Villaescusa-Navarro, M. Viel, D. Alonso, K. K. Datta, P. Bull, and M. G. Santos, *Cross-correlating 21cm intensity maps with Lyman Break Galaxies in the post-reionization era*, *ArXiv e-prints* (October, 2014) [[arXiv:1410.7393](#)].
- [36] K. W. Masui, E. R. Switzer, N. Banavar, K. Bandura, C. Blake, L.-M. Calin, T.-C. Chang, X. Chen, Y.-C. Li, Y.-W. Liao, A. Natarajan, U.-L. Pen, J. B. Peterson, J. R. Shaw, and T. C. Voytek, *Measurement of 21 cm Brightness Fluctuations at  $z \sim 0.8$  in Cross-correlation*, *Astrophysical Journal Letters* **763** (January, 2013) L20, [[arXiv:1208.0331](#)].
- [37] A. Font-Ribera, J. Miralda-Escudé, E. Arnau, B. Carithers, K.-G. Lee, P. Noterdaeme, I. Pâris, P. Petitjean, J. Rich, E. Rollinde, N. P. Ross, D. P. Schneider, M. White, and D. G. York, *The large-scale cross-correlation of Damped Lyman alpha systems with the Lyman alpha forest: first measurements from BOSS*, *Journal of Cosmology and Astroparticle Physics* **11** (November, 2012) 59, [[arXiv:1209.4596](#)].
- [38] N. Jarosik, C. L. Bennett, J. Dunkley, B. Gold, M. R. Greason, M. Halpern, R. S. Hill, G. Hinshaw, A. Kogut, E. Komatsu, D. Larson, M. Limon, S. S. Meyer, M. R. Nolte, N. Odegard, L. Page, K. M. Smith, D. N. Spergel, G. S. Tucker, J. L. Weiland, E. Wollack, and E. L. Wright, *Seven-year Wilkinson Microwave Anisotropy Probe (WMAP) Observations: Sky Maps, Systematic Errors, and Basic Results*, *Astrophysical Journal Supplement* **192** (February, 2011) 14, [[arXiv:1001.4744](#)].
- [39] L. Hui and N. Y. Gnedin, *Equation of state of the photoionized intergalactic medium*, *Monthly Notices of the Royal Astronomical Society* **292** (November, 1997) 27–35, [[astro-ph/9612232](#)].
- [40] N. Y. Gnedin and L. Hui, *Probing the Universe with the Lyalpha forest - I. Hydrodynamics of the low-density intergalactic medium*, *Monthly Notices of the Royal Astronomical Society* **296**

- (May, 1998) 44–55, [[astro-ph/9706219](#)].
- [41] H. Bi and A. F. Davidsen, *Evolution of Structure in the Intergalactic Medium and the Nature of the Ly  $\alpha$  Forest*, *Astrophysical Journal* **479** (April, 1997) 523–532, [[astro-ph/9611062](#)].
- [42] M. Viel, S. Matarrese, H. J. Mo, M. G. Haehnelt, and T. Theuns, *Probing the intergalactic medium with the Ly $\alpha$  forest along multiple lines of sight to distant QSOs*, *Monthly Notices of the Royal Astronomical Society* **329** (February, 2002) 848–862, [[astro-ph/0105233](#)].
- [43] A. Slosar, S. Ho, M. White, and T. Louis, *The acoustic peak in the Lyman alpha forest*, *Journal of Cosmology and Astro-Particle Physics* **10** (October, 2009) 19–24, [[arXiv:0906.2414](#)].
- [44] F. A. Marín, N. Y. Gnedin, H.-J. Seo, and A. Vallinotto, *Modeling the Large-scale Bias of Neutral Hydrogen*, *Astrophysical Journal* **718** (August, 2010) 972–980, [[arXiv:0911.0041](#)].
- [45] K. M. Lanzetta, A. M. Wolfe, and D. A. Turnshek, *The IUE Survey for Damped Lyman-  $\alpha$  and Lyman-Limit Absorption Systems: Evolution of the Gaseous Content of the Universe*, *Astrophysical Journal* **440** (February, 1995) 435–441.
- [46] C. Péroux, R. G. McMahon, L. J. Storrie-Lombardi, and M. J. Irwin, *The evolution of  $\Omega_{HI}$  and the epoch of formation of damped Lyman  $\alpha$  absorbers*, *Monthly Notices of the Royal Astronomical Society* **346** (December, 2003) 1103–1115, [[astro-ph/0107045](#)].
- [47] T. Zafar, C. Péroux, A. Popping, B. Milliard, J.-M. Deharveng, and S. Frank, *The ESO UVES advanced data products quasar sample. II. Cosmological evolution of the neutral gas mass density*, *Astronomy and Astrophysics* **556** (August, 2013) A141, [[arXiv:1307.0602](#)].
- [48] P. Noterdaeme, P. Petitjean, C. Ledoux, and R. Srianand, *Evolution of the cosmological mass density of neutral gas from Sloan Digital Sky Survey II - Data Release 7*, *Astronomy and Astrophysics* **505** (October, 2009) 1087–1098, [[arXiv:0908.1574](#)].
- [49] N. Kaiser and J. A. Peacock, *Power-spectrum analysis of one-dimensional redshift surveys*, *Astrophysical Journal* **379** (October, 1991) 482–506.
- [50] M. McQuinn and M. White, *On estimating Ly $\alpha$  forest correlations between multiple sightlines*, *Monthly Notices of the Royal Astronomical Society* **415** (August, 2011) 2257–2269, [[arXiv:1102.1752](#)].
- [51] M. McQuinn, O. Zahn, M. Zaldarriaga, L. Hernquist, and S. R. Furlanetto, *Cosmological Parameter Estimation Using 21 cm Radiation from the Epoch of Reionization*, *Astrophysical Journal* **653** (December, 2006) 815–834, [[astro-ph/0512263](#)].